

Article

Experimental Exploration of Metal Cable as Reinforcement in 3D Printed Concrete

Freek P. Bos ^{1,*} , Zeeshan Y. Ahmed ¹, Evgeniy R. Jutinov ¹ and Theo A. M. Salet ^{1,2}

¹ Department of the Built Environment, Eindhoven University of Technology, P.O. Box 513, 5600 MB Eindhoven, The Netherlands; z.y.ahmed@tue.nl (Z.Y.A.); evgeniy.jutinov@bam.com (E.R.J.); t.a.m.salet@tue.nl (T.A.M.S.)

² Witteveen+Bos, P.O. Box 233, 7400 AE Deventer, The Netherlands

* Correspondence: f.p.bos@tue.nl; Tel.: +31-(0)40-247-2168

Received: 11 October 2017; Accepted: 8 November 2017; Published: 16 November 2017

Abstract: The Material Deposition Method (MDM) is enjoying increasing attention as an additive method to create concrete mortar structures characterised by a high degree of form-freedom, a lack of geometrical repetition, and automated construction. Several small-scale structures have been realised around the world, or are under preparation. However, the nature of this construction method is unsuitable for conventional reinforcement methods to achieve ductile failure behaviour. Sometimes, this is solved by combining printing with conventional casting and reinforcing techniques. This study, however, explores an alternative strategy, namely to directly entrain a metal cable in the concrete filament during printing to serve as reinforcement. A device is introduced to apply the reinforcement. Several options for online reinforcement media are compared for printability. Considerations specific to the manufacturing process are discussed. Subsequently, pull-out tests on cast and printed specimens provide an initial characterisation of bond behaviour. Bending tests furthermore show the potential of this reinforcement method. The bond stress of cables in printed concrete was comparable to values reported for smooth rebar but lower than that of the same cables in cast concrete. The scatter in experimental results was high. When sufficient bond length is available, ductile failure behaviour for tension parallel to the filament direction can be achieved, even though cable slip occurs. Further improvements to the process should pave the way to achieve better post-crack resistance, as the concept in itself is feasible.

Keywords: 3D concrete printing; reinforcement; entrainment; cable; chain

1. Introduction

In the last few years, 3D printing in the construction industry has enjoyed rapid growth. Additive manufacturing of concrete and cementitious materials (AMoC), in particular, is expanding briskly. After a phase in which showcase objects have been presented that were not intended for structural applications or actual load regimes (for instance: various objects [1], a free-shaped bench [2], a children's castle [3]), and exotic studies were initiated to explore additive manufacturing for extra-terrestrial construction [4–8], we have now entered a phase of (announcements of) the first case-study projects in actual use (a hotel extension [9], an office [10,11], a pedestrian bridge [12], a laboratory [13], a bridge for bicycles and pedestrians [14], a house [15], a motor traffic bridge [16], an office–hotel [17]). Meanwhile, Tay et al. [18] report a steep growth in academic publications in the field since around 2013, not only in number but also in the topics that are being covered. Where these were initially focused on the printing technique, later followed by material analysis, the range of topics has now expanded to include architectural design, literature reviews, data analysis, and so on.

A recurring issue that needs to be resolved when AMoC is used in structural applications is the need to achieve ductility and (flexural) tensile capacity, as the processes that are being applied generally do not yet provide that inherently [19].

In the limited number of projects that have been realised up to now, the strategy generally is to use the printed concrete as lost formwork for conventional reinforced concrete [20,21]. Alternatively, external pre-stressing tendons have been applied to obtain tensile capacity and ductility [14,22]. This strategy, which comes down to avoiding tensile stresses in the concrete, can also be applied in a different way, namely by designing pure compression structures, such as a dome presented by [23].

An altogether different approach has been adopted by Chinese contractor HuaShang Tengda [24] in a project realised in 2016. The reinforced concrete walls of this two-storey house were made by first erecting the conventional reinforcement mesh and subsequently depositing concrete with a Material Deposition Method (MDM)-type machine, with two large forked print nozzles that can simultaneously print on each side of the reinforcement.

However, all these strategies have an important drawback: they seriously limit the level of form-freedom and automation, which are the key selling points of 3D printing. Khoshnevis [25] already recognised that an alternative to conventional reinforcement would be required, and could be incorporated in an automated process without limiting shaping possibilities. Therefore, an embedded coil was suggested that would not only provide longitudinal tensile strength, but also ductility through the layer interfaces, as half of the coil sticks out of the preceding layer. Extensive results on the structural performance of this alternative, however, were not reported.

Another possibility is to include fibers to achieve ductility in the print material itself. Hambach and Volkmer [26] reported significantly improved tensile strengths in mortar samples of several centimeters in size, reinforced with 1 vol % 3–6 mm carbon, glass, and basalt fibers. The 4TU Federation website [27] shows that this option has been explored by others, too.

Hack and Lauer [28] presented the Mesh Mould method, an approach that bears similarities to the one adopted by HuaShang Tengda in the sense that the reinforcement is constructed first and then used as a carrier for the matrix material that is added in a subsequent production step. In the Mesh Mould process, however, the reinforcement is also 3D-printed, thus eliminating the principal problems of form-freedom and automation associated with the HuaShang Tengda process. Initially, the process was developed to print a polymer reinforcement, but as this would have limited functionality due to the low stiffness, the process was further developed to allow automated construction of metal reinforcement as well [29].

One of the techniques that is being developed at the TU Eindhoven (TU/e) builds on the idea of embedding a coil. Bos et al. [30] published the first results using entrained steel cable wires as a reinforcement medium. The current paper presents a more comprehensive study of this concept, intending to:

- develop a suitable entrainment device and determine a suitable medium to act as reinforcement,
- globally establish pull-out characteristics such as bond strength and anchorage length of this medium in printed and cast concrete,
- achieve ductile failure behaviour of printed concrete beams in bending,
- explore any process-characteristic behaviour, aspects, and issues to be considered in further development of this concept.

This paper will go on to describe the reinforcement entrainment device and discuss print process considerations and reinforcement medium selection (Section 2). Some background theory is discussed (Section 3). Then, in two separate sections, the experiments of this study are presented and discussed. Section 4 treats the tensile pull-out test in cast and printed concrete with which initial anchorage characteristics are being established. Subsequently, Section 5 elaborates on the design, manufacturing, and testing of reinforced printed beam elements subjected to four-point bending to assess their

structural performance. The study shows entrained steel cables are a feasible concept to achieve ductility in the print filament direction in printed concrete.

2. Technique and Process of Entraining Reinforcement Cable in 3D Printed Concrete

The 3D concrete printing system adopted by the TU/e has been described extensively by Bos et al. [31]. It consists of an M-Tec Duomix 2000 mixer-pump with a linear displacement pump that feeds concrete by a $\varnothing 25$ mm hose to a $9.0 \times 4.5 \times 2.8$ m³ 4-DOF gantry robot (Figure 1). For this project, the printer head, which previously consisted of a simple stainless steel print nozzle, was expanded with a ‘reinforcement entraining device’ (RED) that allows the introduction of a reinforcement medium to the concrete filament.



Figure 1. 3D concrete printing facility at the TU/e.

The concept of the RED consists of a rotating spool feeding the reinforcement into the printing head where it is introduced in the concrete filament so that an integrated concrete-with-reinforcement filament leaves the print nozzle. This concept was developed into a working prototype following a trial-and-error type process.

In order to succeed, it was clear from the onset that the reinforcement medium would need to meet specific printability requirements, in addition to conventional reinforcing properties. Most importantly, the cross section bending stiffness needed to be as low as possible. This high flexibility was required both for the reinforcement to be able to pass through the print devices and to allow it to follow all 3D freeform lines that can be produced with the concrete filament.

An active feed-system was opted for. A spring-loaded feeder driven by a stepper motor pulls the reinforcement from a spool to direct it into the concrete filament. By incorporating a controllable potentiometer, the rotation frequency can be adjusted to match the reinforcement deposition with the movement speed of the print head so that it equals the length of the print path, straight or curved. The spool used in this study can hold up to 100 m of cable wire. The resulting printer head, equipped with a Reinforcement Entrainment Device (RED), is shown in Figure 2. Recently, an updated version has been developed that can hold more than 2000 m of cable wire, divided over two spools.

Initial tests were performed with $\varnothing 0.35$ mm fishing line and $\varnothing 0.4$ mm steel wire. These proved to have insufficient flexibility and to be too thin, causing them to cut through and pull out of the concrete. Subsequent tests were done with several types of chain (Figure 3). The stepper-motor was equipped with a wildcat chain wheel to feed the chain from the chain locker to the concrete filament, a principle borrowed from the maritime industry to reel in heavy anchor chain. Using chain is promising from a printability perspective: the chain could easily follow any print path. However, the chain geometry and alternating link orientation was expected to have a detrimental effect on the filament quality as the no-slump concrete is not able to properly fill all the gaps formed by the links. Furthermore, the irregular geometry would probably lead to stress concentrations. These combined effects would likely induce early concrete failure. Chain was thus abandoned as a reinforcement alternative.

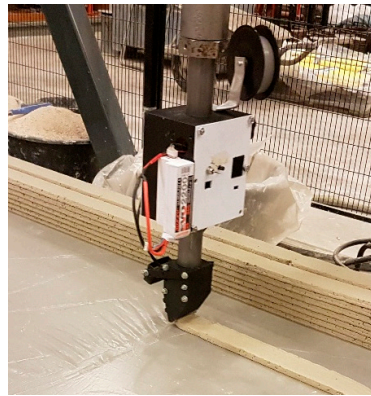


Figure 2. Active reinforcement entrainment device (RED) for cable reinforcement of printed concrete.



Figure 3. Early version of RED, equipped with chain reinforcement.

Finally, three different high-strength steel Bekaert Syncrocord® cables (Table 1) have been tested for printability. These cables are specially developed to combine high tensile strength with great lateral flexibility and are normally used to reinforce synchronous belts. Compared to normal reinforcement steel, their ductility is limited, as the ratio between failure strain and 0.2% offset yield strain is between 1.22 and 1.44. As the cables are constructed out of sets of smaller strands, the actual cable perimeter is larger than the product of the diameter times pi ($p > \pi \cdot d$). The bond stresses in this study are calculated based on the actual perimeter.

Table 1. Cables used as reinforcement.

Property ID	Symbol	Value		
		A	B	C
Name	-	Bekaert Syncrocord Force 0.6	Bekaert Syncrocord Flex 0.9	Bekaert Syncrocord Flex 1.2
Coating	-	Galvanised	Galvanised	Galvanised
Diameter	d [mm]	0.63	0.97	1.20
Perimeter	p [mm]	2.24	5.11	5.87
Linear Density	ρ_{lin} [g/m]	2.30	3.46	5.84
0.2% offset yield strain	$\varepsilon_{0.2}$	1.61%	1.72%	1.90%
0.2% offset yield stress	$f_{0.2}$ [N]	381	1140	1800
Characteristic ultimate tensile strain	ε_{uk}	2.32%	2.10%	2.40%
Characteristic ultimate tensile strength	f_{uk} [N]	420	1190	1925
Axial Tensile Modulus of Elasticity	E_{axi} [GPa]	181.6	178.3	156.8

Using the active feed system, it proved to be possible to print any curvature allowed by the process, with all three cables. Therefore, further research was conducted to establish bond characteristics and the capacity to act as a reinforcement.

3. Cable Reinforcement

To be able to analyse the structural behaviour of steel cables as reinforcement and establish a method to calculate their performance, it is essential to establish their pull-out behaviour. Cables are commonly used as anchoring in grout and concrete in tunneling and mining construction. Geometrically and mechanically, cable bolts are not completely comparable to continuous cables as they feature a bulb near the end, which significantly increases their bearing capacity. Furthermore, with tensile strengths in the order of magnitude of several hundred kN, they are more than 100 times stronger than the cables considered in this study. Their diameters are also much larger, in the order of 2.5–3.5 cm. Hagan et al. [32] note that the influence of critical parameters such as rock mass confinement, cable surface geometry, water:cement ratio, and embedment length on the pull-out resistance are well understood, but that a common testing methodology still needs to be developed for a proper comparison between available cable bolt systems. Chen et al. [33] recently found that in an unconfined condition, the pull-out resistance is proportional to the cable diameter (and thus to the cable perimeter), whereas under confined boundary conditions (i.e., in which radial pressure can develop), this is only partially the case. They also note that the failure mode between confined and unconfined conditions is different (as would be expected): in the former it is characterised by debonding, whereas in the latter failure occurs through sample split. Stress-slippage models have also been developed, such as the tri-linear model proposed by [34]. However, due to the intended function of the cables as reinforcement and the geometrical and mechanical deviations mentioned, their performance is preferable in comparison to conventional bar reinforcement.

The resistance to pull-out behaviour of conventional ribbed reinforcement bars out of NSC (Normal Strength Concrete) may be understood as consisting of a complex combination of at least three phenomena: adhesion, dilatancy, and friction, with the former two, adhesion and dilatancy, occurring before failure and together constituting the bond resistance, and the latter happening after failure and determining the post-failure resistance [35]. The resistance of these three components depends on a number of parameters such as global stress distribution, concrete quality, compaction or bond quality around the reinforcement, and level of confinement [36,37]. Commonly applied models for bond strength, however, are usually primarily based on the concrete quality, with some additional parameters accounting for various conditions. For instance, Eurocode 2 (EC2) [38] defines the design bond strength as:

$$f_{bd} = 2.25\eta_1\eta_2f_{ctd} \quad (1)$$

where η_1 depends on the embedment quality η_2 on the bar diameter, while f_{ctd} is the design tensile strength of the concrete.

The conditions of the concrete applied in 3D concrete printing are rather different from normal cast concrete. Up to and including the current project, the 3DCP research program has used a mortar with strength properties approximately equal to C10/12 grade concrete, but with a maximum grain size of 1 mm, i.e., significantly lower than is usually applied in structural concrete in buildings. Furthermore, the density of printed concrete is lower ($\rho = 2000 \pm 50 \text{ kg/m}^3$) than NSC because the material cannot be compacted after printing.

The EC2 equation for bond stress, however, assumes a number of properties of the reinforcement that are not necessarily valid for the applied cables.

First, the stress-strain behaviour of these cables differs from normal reinforcement steel. According to Eurocode 2, B-grade reinforcement steel, which is commonly used for instance in the Netherlands, yields at $\varepsilon_{yk} = 0.25\%$, and fails at $\varepsilon_{uk} > 5.0\%$, whereas for the applied cables approximately $\varepsilon_{0.2k} = 1.6\text{--}1.9\%$ and $\varepsilon_{uk} = 2.1\text{--}2.4\%$. In other words, the linear elastic strength limit is much higher, and the stiffness is considerably lower than in conventional reinforcement bars (as given by the axial

modulus of elasticity between 157 and 182 GPa, compared to 200 GPa for reinforcement steel bars). Besides the steel quality, this is due to the woven structure of the cable.

Furthermore, the cable surface is smooth. Thus, their pull-out behaviour is likely more comparable to the smooth reinforcement bars that have been used in concrete structures in the past. Since the 1970s, the use of smooth bars has been discontinued in Europe in favour of ribbed bars because of their far superior bond properties caused by the much higher dilatancy resistance. The bond resistance of ribbed bars is found to be approximately 6.6 times as high as for smooth bars [39]. This, naturally, also influences the proportion between adhesive and dilatancy resistance. Since adhesion is found to cause 60% of the bond strength of smooth bars [40], it would only be about 10% for ribbed bars (assuming the bar geometry does not change the concrete-steel adhesion). Experimental research shows bond strengths for smooth rebars of between 1.5 and 2.5 MPa [41,42], which globally corresponds with the results of [39].

Contrary to conventional reinforcement, the cables applied in this research are galvanised (i.e., zinc-coated). Galvanising reinforcement is a technique that has been commonly applied to increase the corrosion resistance of the reinforcement (and thus the structural durability) since the 1930s, especially in saline environments [43]. Galvanised reinforcement steel is governed by various codes, such as ISO 14657 [44] and the ASTM A767 [45]. When galvanised steel comes into contact with uncured concrete, a passivation reaction occurs that consumes about 10 μm of zinc [43]. However, several studies conclude that for all general structural and construction purposes, galvanised coating can be treated as normal reinforcement, as its performance is equal or better [46,47]. Hamid & Mike [48] refer to contradictory results in the literature, but conclude galvanisation has no significant impact on bonding in NSC. A dissenting opinion is voiced by Pernicova et al. [49] who found that the formation of hydrogen during the passivation reaction causes porosity in the surrounding cement thereby deteriorating the bond strength. The severity of this effect was found to be dependent on the pH value of the concrete.

Finally, common bond stress methods assume the concrete matrix can be considered a homogenous material. Applicability often features limits, such as minimal reinforcement diameters and maximum embedment lengths, e.g., 5 times the diameter (5-d [mm]) for the pull out tests of NEN-EN 100080 [50]. However, the applied cables are much thinner while on the other hand the embedment length of 5-d can practically not be achieved in testing, and would also result in a disproportionate influence of discrete effects such as aggregates.

In many ways, the pull-out behaviour of the cables is likely comparable to that of straight steel fibres in terms of proportions between adhesion, dilatancy and friction, considering their small diameter and smooth surface. The parameters that effect these values are mostly similar to those effecting conventional reinforcement, and include concrete matrix composition and strength, water:cement ratio, fiber geometry, length and orientation, fiber surface treatment, and load rate [51–55]. However, even though the pull-out behaviour may be similar, the parameters of interest are usually principally different. For FRC (Fiber Reinforced Concrete), ductility is based the actual pull-out of the fibers (which results in the total debonding energy from adhesion, dilatancy, friction and, depending on the fiber geometry, plastic fiber deformation) therefore the total pull-out energy is an important parameter. In conventional reinforced concrete, on the other hand, ductility is provided by plastic deformation of the rebars while they remain bonded in the concrete on either side of a crack. Hence, the maximum pull-out strength and anchorage length are the primary parameters to determine.

It may be concluded that existing experimental data and models for reinforcement behaviour provide a frame of reference to analyse the cable reinforcement behaviour in 3DCP. However, with regard to geometry, material behaviour of both concrete and steel, as well as the manufacturing method, significant differences exist that call for caution when interpreting results.

4. Pull-Out Test

The bond behaviour of three types of cable reinforcement was investigated by pull-out tests on cast and printed concrete samples with different embedment lengths.

4.1. Method

4.1.1. Specimen Preparation—Cast

For the pull-out tests on cast concrete specimens, rectangular blocks were cast around cables, that were slightly pre-stressed in order to guarantee their straightness, and compacted on a vibrating table for 10 s. The same 3DCP print mortar, described by [31], was used for the cast and the printed specimens. Unpublished test results on compressive strength, tensile strength, and modulus of elasticity have shown these properties to be in the range of C20/25 when cast and printed, loaded in compression, but more comparable to C10/12 or C12/15 when printed, loaded in tension. It should be noted, however, that the material is not completely comparable to conventional concrete, among others because the maximum particle size is only 1 mm.

After casting, the specimens were wrapped in foil to prevent dehydration, and left to cure for 14 days at ambient lab temperature. Several series of specimens were produced, with three different cables (A, B, and C—see Table 1) and 2 different embedment lengths $l_{cs} = 15$ and 35 mm. The results of an initial test series with $l_{cs} = 25$ mm were abandoned because of deviating concrete quality, which led to incomparable results. Throughout the experimental part of the research, each series consisted of five specimens. Consequently, 30 cast specimens were prepared and tested.

4.1.2. Specimen Preparation—Printed

The printed specimens were taken from three subsequently printed objects (Figure 4a). In each object, the reinforcement cable (A, B, and C respectively) is in the bottom layer (Figure 4b). Still in the wet state, the printed concrete filament was cut with a custom designed U-shape device to obtain each specimen (Figure 4c). The excess material on each side of the cut was removed in order to obtain protruding cables that could be used to apply loading and measurement equipment. Besides three different cables, specimens of three different embedment lengths $l_{cs} = 15$, 25 and 35 mm were produced (resulting in a total of 45 specimens). The specimens were left to cure under foil on the print table for one day, and then submerged in water until testing at 14 days old. Table 2 provides an overview of the pull-out test specimen series.

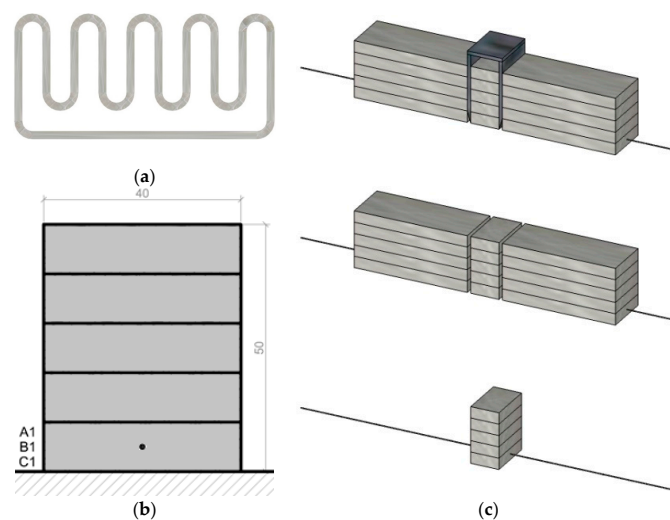


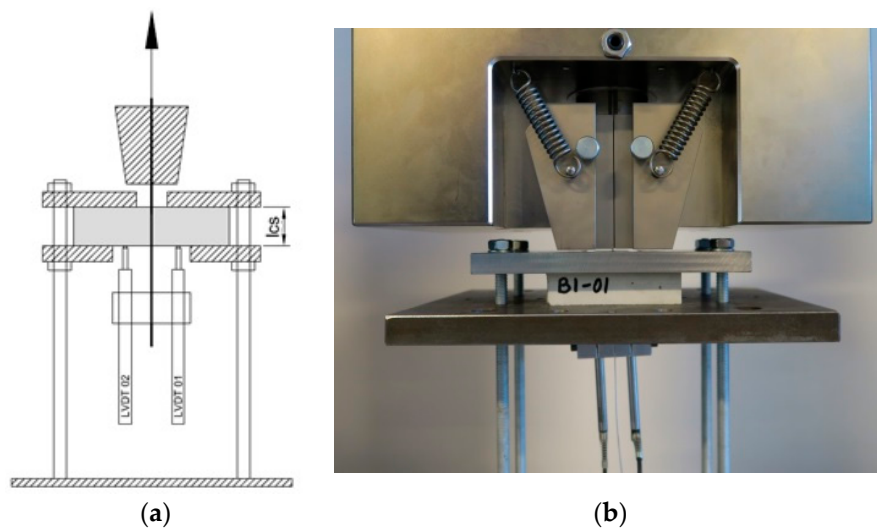
Figure 4. (a) Print path and (b) transverse section of printed objects from which the respective specimens were obtained; (c) cutting and stripping of printed specimens.

Table 2. Specimen series overview.

Series	No. of Specimens	Concrete Manufacturing	Cable	l_{cs} [mm]
C15A	5	Cast	A	15
C15B	5	Cast	B	15
C15C	5	Cast	C	15
C35A	5	Cast	A	35
C35B	5	Cast	B	35
C35C	5	Cast	C	35
P15A	5	Printed	A	15
P15B	5	Printed	B	15
P15C	5	Printed	C	15
P25A	5	Printed	A	25
P25B	5	Printed	B	25
P25C	5	Printed	C	25
P35A	5	Printed	A	35
P35B	5	Printed	B	35
P35C	5	Printed	C	35

4.1.3. Experimental Set-Up

The specimens were subjected to a displacement controlled pull-out test at 0.5 mm/min, performed in an Instron universal test rig equipped with a 5 kN load cell. The cable slip was recorded by averaging measurement results of 2 LVDT's fitted to the cables at the bottom side of the specimen as shown in Figure 5a–d. The test rig grip was positioned as close to the specimen as possible and its displacement was also recorded.

**Figure 5.** Cont.

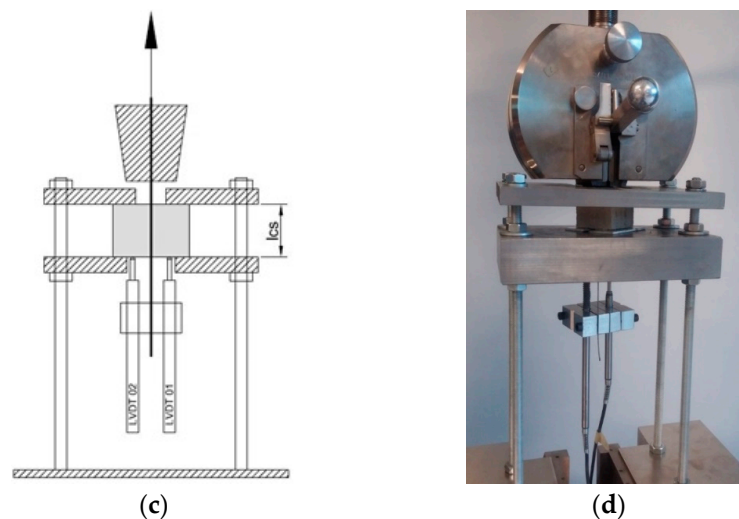


Figure 5. Test set-up for the cast (a,b) and printed (c,d) specimens.

4.2. Results

Figures 6a,b and 7a–c show load-slip curves per embedment length of representative specimens from each series (chosen to illustrate their typical performance) of the cast and printed specimens respectively. Of each specimen series, the adhesive bond strength (taken as the end of the initial linear force-displacement path; F_{adh} , δ_{adh}) and the ultimate bond strength (F_u , δ_u) are listed in Table 3, the former assumed to be determined solely by the cable-matrix adhesion, and the latter by a combination of adhesive bond, dilatancy, and/or friction. The corresponding shear stresses have been calculated from the cable perimeters listed in Table 1. These are average shear stresses, i.e., $\tau_u = F_u / p l$. Although it is known that the shear stress distribution will not be distributed equally along the cable length, but rather peak at the top side where the load is introduced, this approach is commonly applied in reinforcement-matrix pull-out analyses and therefore maintained here as well. All specimens in both the cast and printed series failed on cable pull-out, except for the C35A series, in which gradual breakage of individual strands within the cable introduces failure.

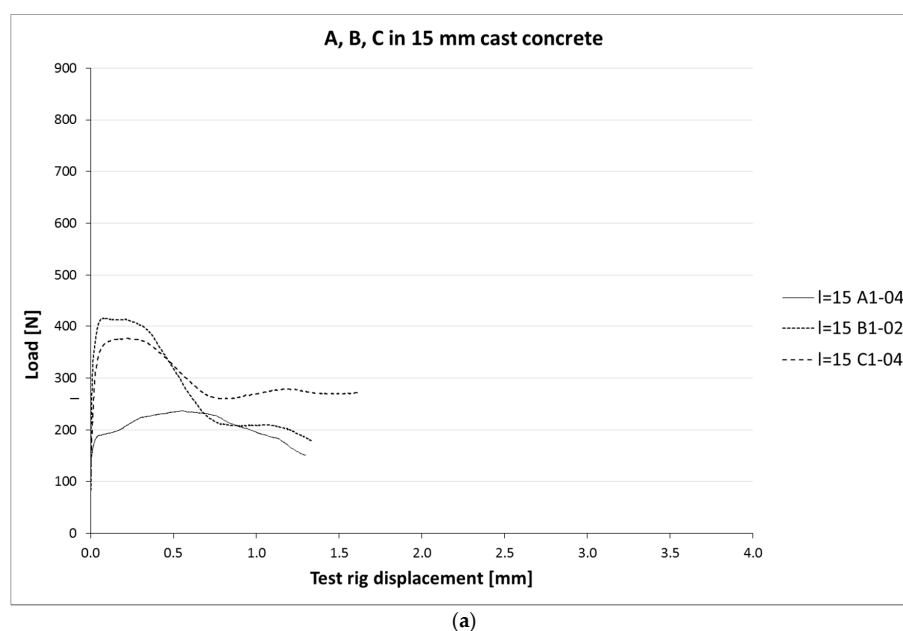
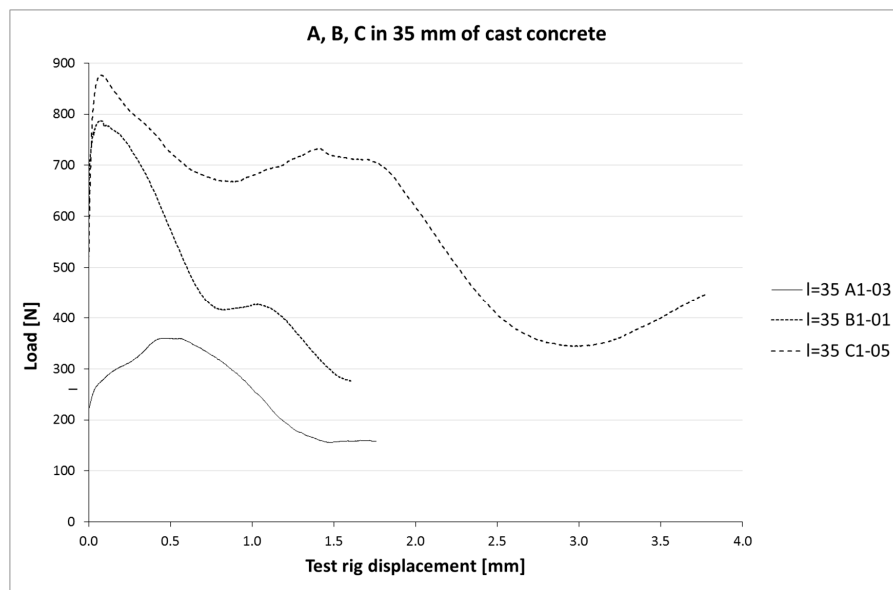
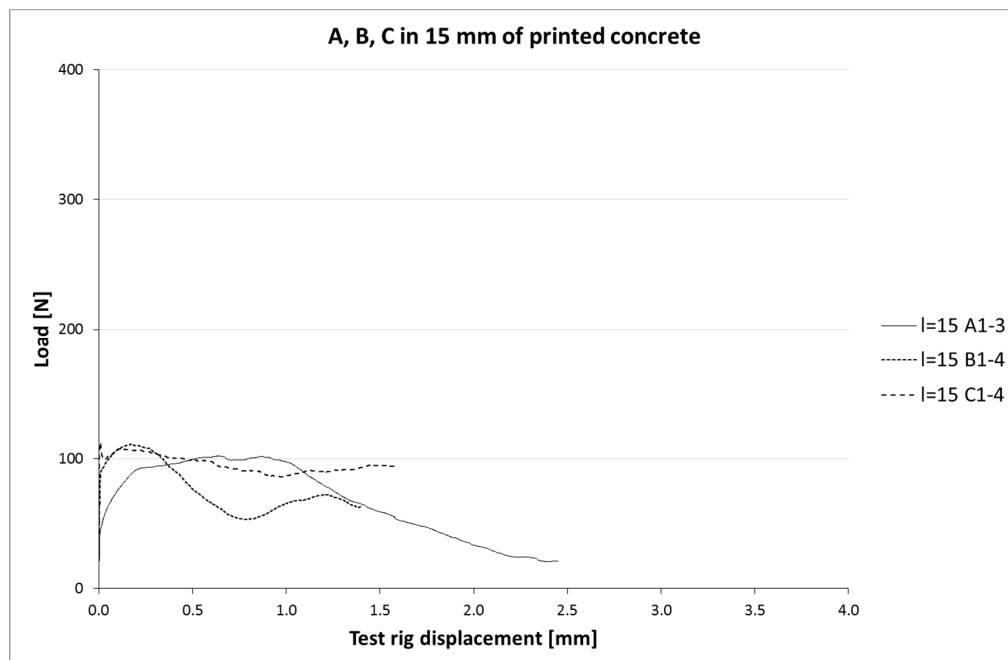


Figure 6. Cont.



(b)

Figure 6. (a) Load-slip curves of pull-out tests of cast samples with $l_{CS} = 15$ mm. For each series, one curve is shown (for reasons of clarity), considered representative for that particular series. It should be noted that the individual behaviour can differ significantly, as is also clear from the coefficients of variation. (b) Load-slip curves of pull-out tests of representative cast samples with $l_{CS} = 35$ mm.



(a)

Figure 7. Cont.

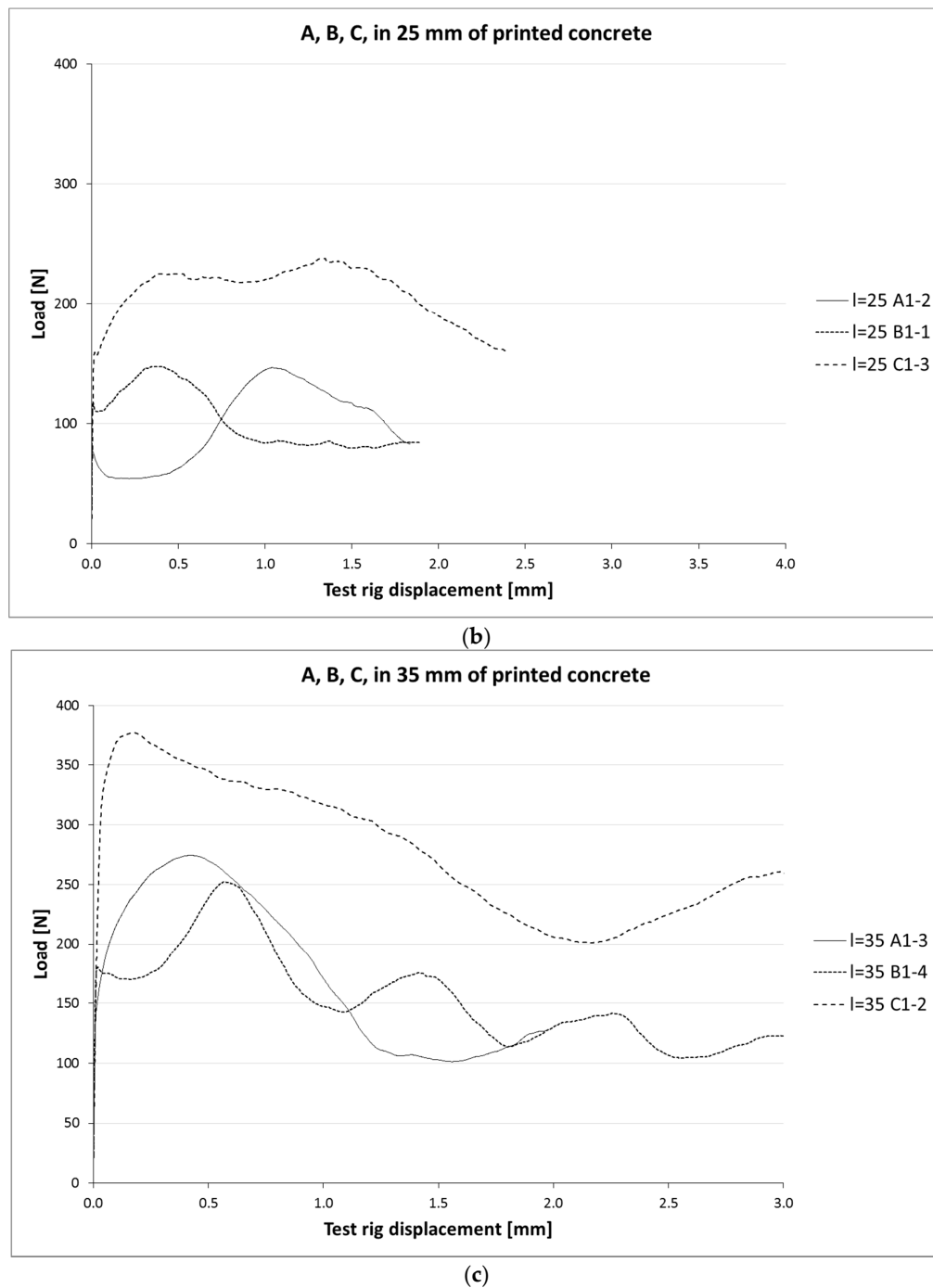


Figure 7. (a) Load-slip curves of pull-out tests of printed samples with $l_{CS} = 15$ mm. For each series, one curve is shown (for reasons of clarity), considered representative for that particular series. It should be noted that the individual behaviour can differ significantly, as is also clear from the coefficients of variation. (b) Load-slip curves of pull-out tests of representative printed samples with $l_{CS} = 25$ mm; (c) Load-slip curves of pull-out tests of representative printed samples with $l_{CS} = 35$ mm.

Table 3. Specimen series results.

Series	F_{adh} [N]; CoV	τ_{adh} [MPa]	F_u [N]; CoV	τ_u [MPa]	τ_{adh}/τ_u
C15A	139.03; 17%	4.15	238.83; 27%	7.12	0.58
C15B	330.92; 10%	4.31	417.50; 10%	5.44	0.79
C15C	327.12; 17%	3.72	396.95; 14%	4.51	0.82
C35A	245.30; 6%	3.13	347.76; 9%	4.44	0.70
C35B	688.66; 10%	3.85	826.44; 11%	4.62	0.83
C35C	505.08; 28%	2.46	995.87; 18%	4.85	0.51
P15A	48.62; 17%	1.45	79.57; 22%	2.37	0.61
P15B	80.80; 30%	1.05	102.02; 29%	1.33	0.79
P15C	100.54; 24%	1.14	113.62; 39%	1.29	0.88
P25A	83.41; 19%	1.49	173.24; 31%	3.10	0.48
P25B	142.67; 34%	1.12	177.49; 38%	1.39	0.81
P25C	188.45; 13%	1.28	321.70; 36%	2.19	0.58
P35A	143.20; 18%	1.83	242.40; 27%	3.10	0.59
P35B	163.40; 11%	0.91	253.88; 8%	1.42	0.64
P35C	354.74; 4%	1.73	409.63; 6%	1.99	0.87

Figure 8 shows a typical cast sample after testing. In Figure 9, a part of the printed object is shown, transversely broken open after curing. This was not a specimen, but rather a part of the object not used for the samples. It shows that the irregularities (voids, bubbles, etc.) around the cable positioning are much more severe than in the cast specimens. This difference in matrix quality is caused by the printing process, which, unlike the casting process, does not include compaction on a vibrating table.

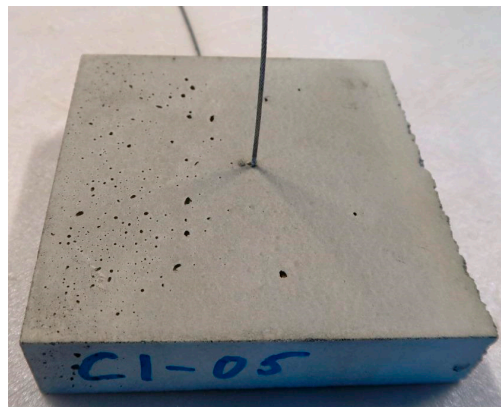
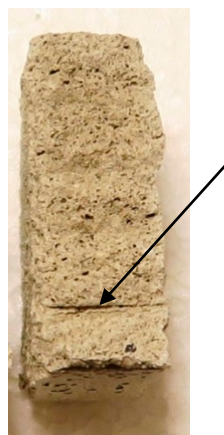
**Figure 8.** Representative cast specimen after testing.**Figure 9.** Transversally broken part of print object (not specimen) to show voids around cable shaft.

Figure 10 shows the development of average adhesive bond stress over embedment length for cast and printed specimens. In Figure 11, the average adhesive bond stresses are compared.

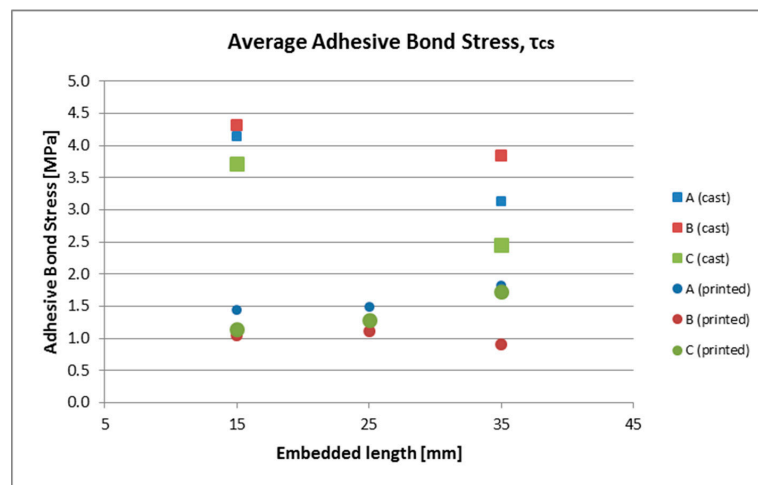


Figure 10. Development of average adhesive bond stress over increasing embedment length.

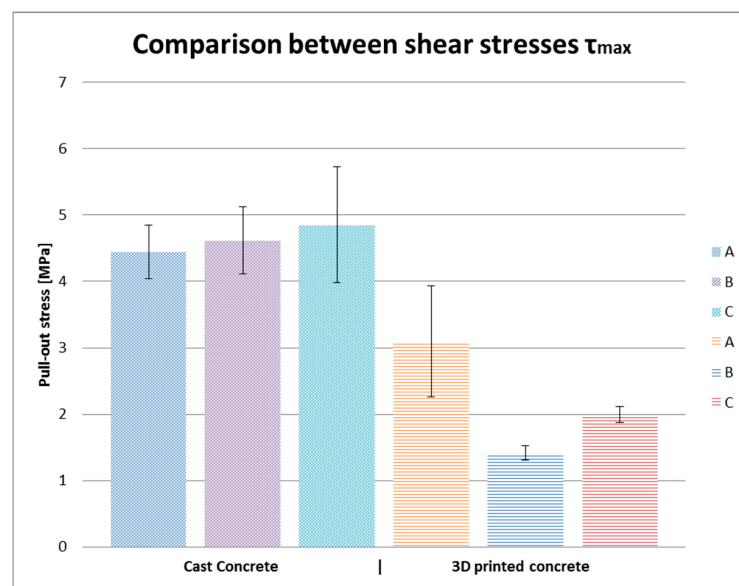


Figure 11. Comparison of average ultimate bond stress in cast and printed specimen.

As failure in all printed specimens occurs through cable pull-out and the results show no clear trend in bond strength development over embedment length, basic anchorage lengths can be calculated from the cable data (Table 1) and the bond stress, averaged per cable type over the three investigated embedment lengths: $l_{\text{anchorage}} = F / \tau_{\text{max}} p$. These are listed in Table 4. Anchorage lengths have been calculated based both on adhesive and ultimate bond stress.

Table 4. Basic anchorage lengths for applied cables in printed concrete, based on adhesive ($l_{\text{anchorage,adh}}$) and ultimate ($l_{\text{anchorage,u}}$) bond stress.

Cable Type	F_u [N]	P [mm]	$\tau_{\text{max,ave 15/25/35}}$ [MPa]	$l_{\text{anchorage,adh}}$ [mm]	$l_{\text{anchorage,u}}$ [mm]
A	420	2.24	2.86	117.9	65.6
B	1190	5.11	1.38	217.3	161.7
C	1925	5.87	1.82	237.1	179.9

4.3. Discussion

4.3.1. Cast Specimens

The load-slip curves of the cast specimens show a clear steep branch representing the adhesive bond (the displacement of the cable at the bottom side of the specimens is almost 0), and a consecutive branch with partial bonding and dilatancy. After the maximum bond strength is reached, a gradual degrading branch starts caused by friction. It should be noted that the adhesive branch for the C cables is less steep. This is caused by the structure of that cable, with a core and a mantle.

In neither of the cast specimen series does the embedded length influence the ultimate bond stress. Although at first glance there seems to be an influence in the A-cable specimens (Table 3), this difference is caused by a change in failure mechanism (pull-out versus gradual strand breakage in the cable), not by a change in cable-to-matrix bond strength.

The adhesive bond stress on the other hand, seems to decrease slightly with increasing embedded length (Figure 10). This might be explained from the real stress distribution. The difference in adhesive stress on the load side of the cable and the non-load side, will be higher for longer embedment lengths, resulting in a decreased average stress. However, the effect is minor over the investigated length, whereas the scatter is considerable, and should therefore be treated cautiously.

The ratio τ_{adh}/τ_u ranges from 0.6 to 0.8. As discussed previously, this is comparable to values found for smooth rebar, where the adhesive bond accounts for around 60% of the ultimate bond strength. In absolute terms, the maximum bond stress is somewhat higher than expected for smooth rebar.

The differences in adhesive and maximum bond stresses between the series are considerable and do not show a consequent pattern. An explanation, therefore, remains elusive. The scatter in results is also substantial, but does not seem to depend on embedded length or cable type.

4.3.2. Printed Specimens

Like the cast specimens, the printed specimens show a clear adhesive branch that is less steep with the C cables. After the adhesive strength is reached though, a drop in load occurs in about 40% of the specimens, indicating a sudden release of the cable that is less counteracted by dilatancy. The inferior concrete matrix quality, as shown in Figure 9, is likely the culprit. In the other cases, the behaviour after the adhesive branch is comparable to that of the cast specimens.

Contrary to the cast specimens, no clear trend (decreasing or increasing) in the adhesive bond stress over increasing embedment length can be noticed. Again, the reduced matrix quality is likely to blame: any increase in shorter embedment lengths due to an altered stress distribution is annulled by a relatively increasing effect of matrix defects.

The τ_{adh}/τ_u ratio is comparable to the cast specimens, but can run to slightly higher values from 0.6 to 0.9 (in the latter case the contribution of dilatancy to the overall bond resistance has become almost negligible). Both the adhesive and ultimate bond stress are significantly lower than for the cast specimens—again caused by the inferior matrix quality. Nevertheless, the ultimate bond strength is still close to what could be expected of smooth rebar. The scatter in results for cable type A is clearly larger than for cable types B and C. The reason for this is unclear.

4.3.3. Previous Research

Finally, it is noted that the anchorage lengths calculated in Table 4 can, globally, be matched with the experimental results presented by [30] of reinforced printed beams, loaded in four-point bending. In those tests, the distance between the load and support points on either side of a beam were 160 mm, while the cantilever over the support point was 35 ± 5 mm, resulting in a total anchorage length of 195 ± 5 mm when calculating from one support point. All specimens with C-cables failed by cable slip usually from a crack that originated in the four-point bending center span within several centimeters of a support point, i.e., <240 mm from the edge. The calculated anchorage length for C cables is 180 mm

based on maximum bond stress, but 237 mm based on adhesive bond stress. This seems to suggest the adhesive bond stress should be maintained to determine the anchorage length. Exceeding the adhesive strength likely causes damage (e.g., gradual debonding) that will over longer lengths result in a lower maximum bond stress (in such a case the bond strength would be independent of embedment length if the adhesive bond stress is exceeded). On the other hand, none of the A-cable specimens in that study failed by slip, which matches with the anchorage length of 118 mm (based on adhesive bond) found in the current study.

4.4. Conclusions on Pull-Out Test

The pull-out tests have shown that considerable ultimate bond strengths (better than smooth rebar) can be achieved between the cables and cast concrete. Additionally, reasonable ultimate bond strengths (comparable or slightly worse than smooth rebar) can be achieved between the cables and printed concrete. However, the difference between the bond strength with cast and printed concrete is significant. This is likely caused by differences in the concrete matrix quality. Improvement of the bond strength in printed concrete should, therefore, be pursued. An additional advantage is likely to be a reduced scatter in strength.

5. Four-Point Bending Test

5.1. Method

5.1.1. Specimen Design

The beam specimen design included cables in each layer, as that is a likely situation in printed objects in which this technique is applied. Furthermore, the dimensions were chosen so that, from a simple analytical calculation, the failure moment M_u exceeds the crack moment M_{cr} . For the concept to be comparable to conventional reinforcement in terms of performance, $M_u > M_{cr}$ is a precondition.

Bos et al. [30] show that simple mechanical section calculations for conventional reinforcement to determine the failure moment, at least globally also apply to cable reinforced concrete. The failure moment was thus calculated from:

$$M_u = F_{u,cable} \times n \times z_{ave}, \text{ where} \quad (2)$$

$F_{u,cable}$ = the ultimate force in a cable, taken from Table 1.

n = the number of cables

z_{ave} = the average internal lever arm, taken as $z_{ave} = 0.9 \times d_{ave}$, with d_{ave} = the average distance from the reinforcement heart line to the beam top. Based on [30], each reinforcement cable is assumed to be positioned 8 mm from the bottom of the respective layer. The layer thickness itself considered to be $h_{layer} = 11$ mm, the width $b = 50$ mm.

The crack moment was determined by:

$$M_{cr} = f_{cm} W = f_{cm} b h^2 / 6. \quad (3)$$

This simplified equation is applicable as the influence of the cables on the crack resistance is negligible (<1%). For the concrete flexural strength, $f_{cm} = 1.9$ MPa was applied. This value is based on unpublished tensile tests and has been known to deviate. It should therefore be considered an approximation.

The beam length and span proportions were selected based on the test rig dimensions and calculated anchorage lengths from the pull-out tests. Figure 12 presents the four-point bending scheme. The sum of the cantilever c and the load-to-support distance a should exceed the anchorage length: $a + c > l_{anchorage}$.

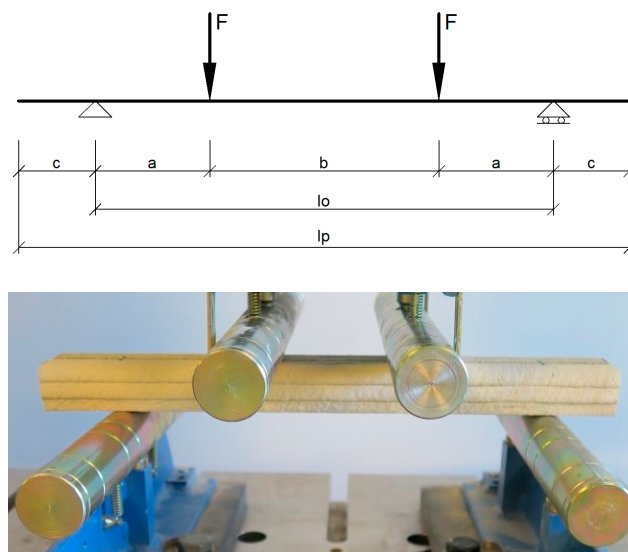


Figure 12. Four-point bending test scheme.

With a single cable A in each layer and the available print nozzle, it proved difficult to achieve dimensions in which the failure moment would be higher than the crack moment. This requirement was therefore abandoned for cable type A (not for the other two). Obviously, this indicates that cable A is less suitable than cables B and C as replacement of conventional reinforcement in printed concrete.

These considerations led to a beam section of three layers in height (Figure 13), 1000 mm overall length, a support span of 900 mm and a load span of 450 mm. The analytically calculated crack and failure moments are given in Table 5 with the experimental results.

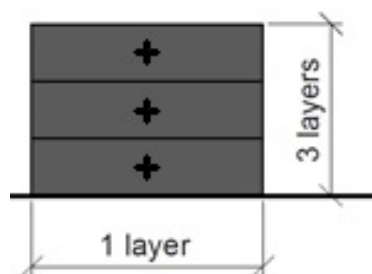


Figure 13. Beam specimen section design.

Table 5. Four-point bending test results.

Beam Specimen	M_{cr} [10^3 Nmm]	M_u [10^3 Nmm]	M_u/M_{cr}	No. Cracks	Failure Mode
<i>Analytical estimate</i>	17.1	13.6	80%	-	<i>Cable break</i>
A1	19.0	14.1	74%	1	Cable break
A2	21.0	18.0	86%	1	Cable break
A3	17.6	15.3	87%	1	Cable break
Average	19.2	15.8	82%	-	-
Coeff. of variation	9%	13%	9%	-	-
<i>Analytical estimate</i>	17.1	38.6	304%	-	<i>Cable break</i>
B1	18.8	17.6	93%	2	Cable slip
B2	23.9	21.1	88%	1	Cable slip
B3	18.1	15.0	83%	2	Max. defl.

Table 5. Cont.

Beam Specimen	M_{cr} [10^3 Nmm]	M_u [10^3 Nmm]	M_u/M_{cr}	No. Cracks	Failure Mode
B4	16.8	29.8	177%	3	Cable slip
B5	15.2	15.1	99%	2	Max. defl.
B6	17.4	11.5	66%	2	Max. defl.
Average	20.3	18.4	101%	-	-
Coeff. of variation	16%	35%	39%	-	-
<i>Analytical estimate</i>	<i>17.1</i>	<i>62.4</i>	<i>491%</i>		<i>Cable break</i>
C1	15.3	27.5	179%	1	Cable slip
C2	14.9	21.4	144%	2	Cable slip
C3	16.0	27.5	172%	2	Cable slip
C4	16.9	22.6	134%	2	Cable slip
C5	12.8	15.1	118%	2	Cable slip
Average	15.2	22.8	149%	-	-
Coeff. of variation	10%	23%	17%	-	-

5.1.2. Specimen Preparation

The four-point bending specimens were taken from three subsequently printed objects. Each object is three layers high; reinforcement cable (A, B, and C, respectively) are entrained in each layer. After printing, the objects were covered in foil for one day, subsequently submerged in water, and left to cure for 28 days. The long straight sides were then sawed into beams with a diamond saw. Three specimens with cable A were tested, six with cable B and five with cable C.

5.2. Results

The test results of the four-point bending tests are listed in Table 5. The corresponding load-displacement curves are shown in Figures 14–16.

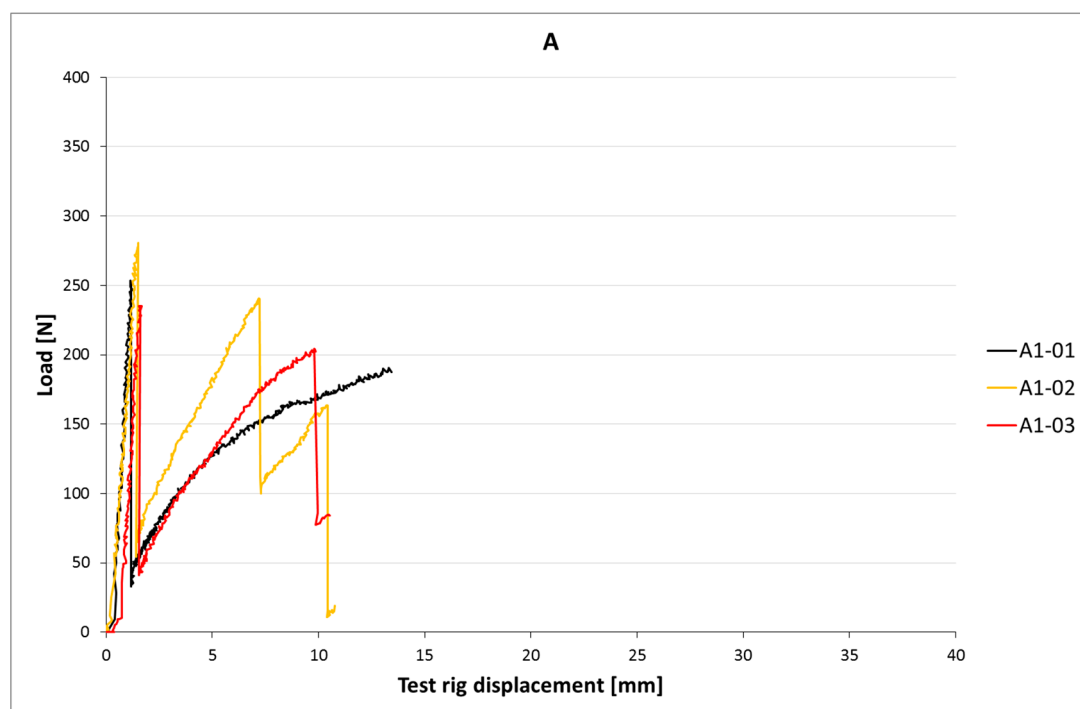


Figure 14. Load-displacement curves of printed beams with A-type cable.

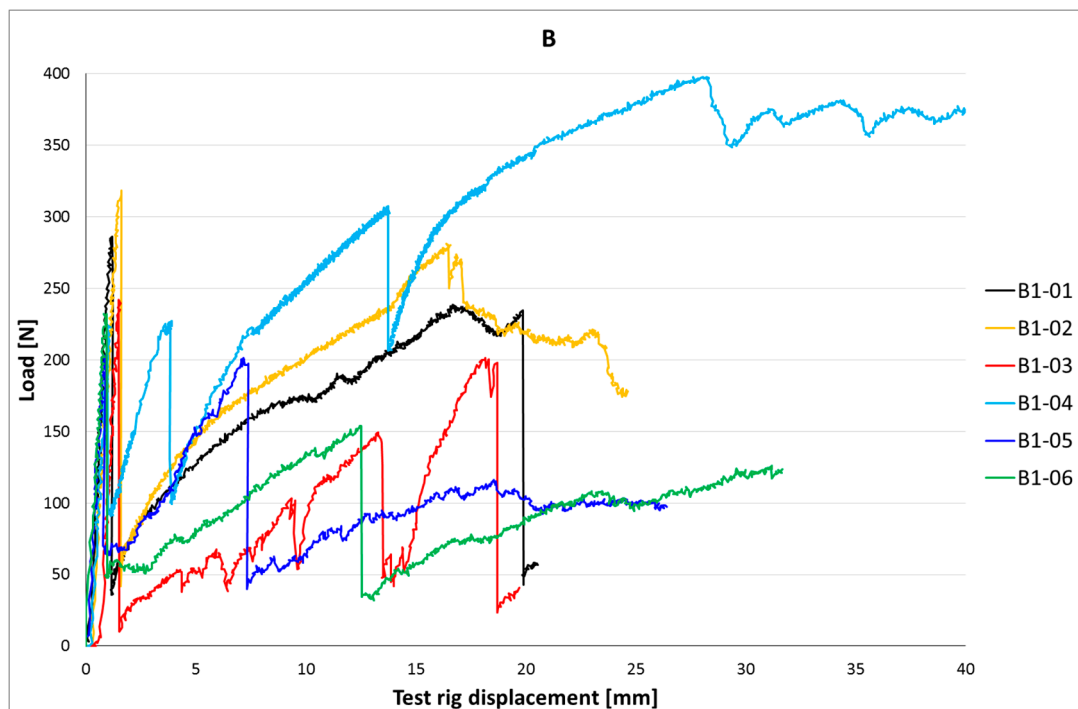


Figure 15. Load-displacement curves of printed beams with B-type cable.

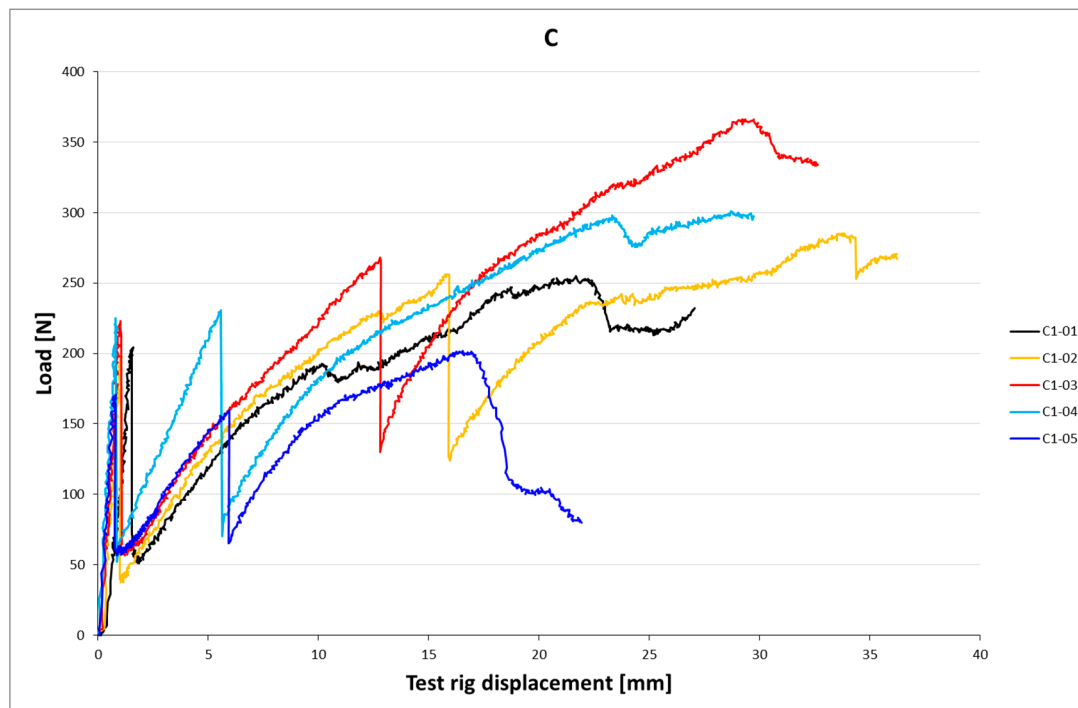


Figure 16. Load-displacement curves of printed beams with C-type cable.

5.3. Discussion

The crack moment of the beams with cable type A (19.2 Nm) is slightly higher than the analytically calculated value (17.1 Nm). This could be caused by geometrical deviations or the actual concrete flexural strength.

Failure occurs by cable breakage, as desired. The failure moment is practically equal to the calculated value. This confirms the suitability of analytical analysis methods for conventional concrete also for printed concrete with cable reinforcement. As expected, the failure moment does not exceed the crack moment. This fits with the single localised crack that occurs.

The beams with cable B also crack at a moment that is somewhat higher (20.1 Nm) than the analytical value. Contrary to the A-cable beams, however, the failure moment is significantly lower than the analytical result. On average, it barely exceeds the crack moment, is this entirely due to one specimen outperforming the rest (B4, reason unclear). The cause for this discrepancy is the failure mode. Instead of cable breakage, cable slip occurs. This also results in a higher scatter for M_u (35%, or 22% without specimen B4). Considering the previous results ([30]; in this study on cable reinforced beams, cable breakage of B-type cables occurred) and the calculated anchorage length ($l_{adh} = 217$; Table 4), this was unexpected. The inferior bond quality could be caused by the low number of layers in this specimen design. In the pull-out specimens, as well as the beam specimens of [30], the internal pressure from self-weight was larger due to the higher number of layers printed. This likely resulted in better compaction of the concrete around the reinforcement cables. Together, these results show the potential of cable reinforcement, but also the need to better control the cable printing process to achieve more constant results.

The crack moment of the C-cable specimens is significantly lower than that of the A- and B-cable beams, and lower than the analytical value as well. Again, deviations in concrete geometry and strength are the likely cause. The failure moment, on the other hand, is significantly higher than both the crack moment and the failure moments of the other beams, due to the higher reinforcement strength. Still, it does not come near the analytical value as here, too, failure is induced by cable slip instead of cable breakage. In the study of [30], this was also experienced, even though the pull-out tests indicate that cable breakage should occur as the anchorage length exceeds l_{adh} (237 mm).

In the B- and C-cable beams unexpected failure caused by cable slip occurs. The internal pressure may influence the adhesion. An additional cause could be the peak stresses at the load side of the cable. They will reach a certain value that may cause gradual debonding that will induce eventual failure regardless of the anchorage length. The low concrete strength and the matrix defects that occur particularly to the underside of the cable, may cause this effect to occur before the cable has had the chance to activate sufficient anchorage length to break itself. The pull-out tests did not signal such an effect, but the forces in those tests stayed well below the strengths of cables B and C. This effect might only occur at larger embedment lengths. Further research is required.

The four-point bending tests have shown that the presented in-print reinforcement method is feasible and can result in considerable post-crack resistance, similar to conventionally reinforced concrete. However, premature bond failure results in underachievement of the cables and high scatter. Thus, improvement of the concept is necessary.

In comparing cables A, B, and C, it is apparent that cable A currently provides the most predictable structural behaviour, but is nevertheless less suitable as its absolute strength is limited. Only when the concrete filament size is significantly reduced or the number of cables per layer is increased, can this cable provide sufficient strength. Cables B and C, on the other hand, provide sufficient strength but suffer from adhesion problems. Process improvements should eliminate this in the future.

6. Summary and Conclusions

Directly entrained cables have been introduced as a reinforcement method for 3D-printed concrete. A device was presented to entrain these cables directly during printing, resulting in a single automated manufacturing process. Two experiments have been conducted: a pull-out test on cast and printed concrete with different embedment lengths and three types of reinforcement cables, and a four-point bending test on printed beams with the same three cables.

The pull-out tests showed the bond strength of cables in cast concrete is low compared to conventional ribbed rebar, but somewhat higher than that of smooth rebar. In printed concrete,

the bond strength was considerably lower than in cast concrete, and towards the lower end of what would be expected of smooth rebar. The concrete matrix showed substantial defects, particularly underneath the reinforcement cable.

Subsequently, the four-point bending tests showed significant post-crack resistance can be achieved with the B- and C-type cables. However, failure of the respective specimens was governed by cable slip, which was not expected based on the pull-out tests. This increases the scatter, and results in failure moments (far) below the analytically determined potential based on cable breakage. In the A-cable beams, cable slip did not occur. Rather, failure was induced by cable breakage resulting in failure moments close to the analytically determined values. Nevertheless, these were below the crack moment due to the limited cable strength.

The bending tests confirmed the suitability of analytical analysis methods to determine the resistance of conventional concrete also for printed concrete with cable reinforcement, at least to obtain global estimates on moment resistance.

The concept of directly entrained cable reinforcement has been shown to be a feasible reinforcement method that can achieve performances similar to conventional reinforcement in cast concrete. However, effort needs to be taken to improve the bond strength and scatter on the B- and C-type cables, so that their failure strengths can be reached before cable slip occurs. The A-type cable works well, but does not seem to be strong enough for practical applications.

Acknowledgments: The assistance in the 3DCP research of Master track students Structural Design at the TU/e Department of the Built Environment is highly valued. The TU/e research program on 3DCP is co-funded by a partner group of enterprises and associations, which as of the date of writing consisted of (alphabetical order) Ballast Nedam, BAM Infraconsult bv, Bekaert, Concrete Valley, CRH, Cybe, Saint-Gobain Weber Beamix, SGS Intron, SKKB, Van Wijnen, Verhoeven Timmerfabriek, and Witteveen+Bos. Their support is gratefully acknowledged. In particular, the authors would like thank SG Weber Beamix and Bekaert NV for supplying the printing concrete and reinforcement cables, respectively.

Author Contributions: The research was conceived by and performed under supervision of Theo A. M. Salet and Freek P. Bos. The reinforcement entrainment device was developed by Zeeshan Y. Ahmed. The experimental work was performed by Evgeniy R. Jutinov. The data were analyzed by Freek P. Bos, who also prepared the manuscript.

Conflicts of Interest: The authors declare no conflict of interest.

References

1. Khoshnevis, B.; Russel, R.; Kwon, H.; Bukkapatnam, S. Contour Crafting Large Prototypes. *IEEE Robot. Autom. Mag.* **2001**, *8*, 33–42. [[CrossRef](#)]
2. Lim, S.; Le, T.; Webster, J.; Buswell, R.; Austin, S.; Gibb, A.; Thorpe, T. Fabricating Construction Components Using Layer Manufacturing Technology. In Proceedings of the Global Innovation in Construction Conference (GICC'09), Loughborough, UK, 13–16 September 2009.
3. Totalkustom. Available online: <http://www.totalkustom.com/3d-castle-completed.html> (accessed on January 2016).
4. Khoshnevis, B.; Bodiford, M.; Burks, K.; Ethridge, E.; Tucker, D.; Kim, W.; Toutanji, H.; Fiske, M. Lunar contour crafting—A novel technique for ISRU-based habitat development. In Proceedings of the 43rd AIAA Aerospace Sciences Meeting and Exhibit, Aerospace Sciences Meetings, Reno, NV, USA, 10–13 January 2005. [[CrossRef](#)]
5. Khoshnevis, B.; Zhang, J. Extraterrestrial construction using contour crafting. In *Solid Freeform Fabrication Proceedings*; University of Texas: Austin, TX, USA, 2012; pp. 250–259.
6. Colla, V.; Dini, E. Large scale 3D printing: From deep sea to the moon. In *Low-Cost 3D Printing, for Science, Education & Sustainable Development*; Canessa, E., Fonda, C., Zennaro, M., Eds.; ICTP: Trieste, Italy, 2013; pp. 127–132.
7. Cesaretti, G.; Dini, E.; De Kestelier, X.; Colla, V.; Pambaguian, L. Building components for an outpost on the Lunar soil by means of a novel 3D printing technology. *Acta Astronaut.* **2014**, *93*, 430–450. [[CrossRef](#)]
8. Joshi, S.C.; Sheikh, A.A. 3D printing in aerospace and its long-term sustainability. *Virtual Phys. Prototyp.* **2015**, *10*, 175–185. [[CrossRef](#)]

9. 3ders. Available online: <http://www.3ders.org/articles/20150909-lewis-grand-hotel-andrey-rudenko-to-develop-worlds-first-3d-printed-hotel.html> (accessed on 26 September 2017).
10. Cnet. Available online: <http://www.cnet.com/news/dubai-unveils-worlds-first-3d-printed-office-building> (accessed on January 2016).
11. Mediaoffice. Available online: <http://mediaoffice.ae/en/media-center/news/23/5/2016/3d-printed-office-building.aspx> (accessed on January 2016).
12. 3ders. Available online: <http://www.3ders.org/articles/20161214-spain-unveils-worlds-first-3d-printed-pedestrian-bridge-made-of-concrete.html> (accessed on 26 September 2017).
13. 3ders. Available online: <http://www.3ders.org/articles/20170602-cybe-construction-completes-3d-printing-of-168-sq-m-rdrone-laboratory-in-dubai.htm> (accessed on 26 September 2017).
14. De Ingenieur. Available online: <https://www.deingenieur.nl/artikel/betonnen-fietsbrug-uit-de-printer> (accessed on 26 September 2017).
15. 3ders. Available online: <http://www.3ders.org/articles/20170213-3d-printing-construction-company-apis-cor-prints-37-m2-house-near-moscow-plans-global-expansion.html> (accessed on 26 September 2017).
16. Cementonline. Available online: <https://www.cementonline.nl/proefstuk-eerste-3d-geprinte-autobrug-sterker-dan-verwacht> (accessed on 24 September 2017).
17. 3ders. Available online: <http://www.3ders.org/articles/20170907-3d-printed-concrete-office-hotel-coming-to-copenhagen.html> (accessed on 24 September 2017).
18. Tay, Y.W.D.; Panda, B.; Paul, S.C.; Mohamed, N.A.N.; Tan, M.J.; Leong, K.F. 3D printing trends in building and construction industry: A review. *Virtual Phys. Prototyp.* **2017**, *12*, 261–276. [CrossRef]
19. Salet, T.A.M.; Bos, F.P.; Wolfs, R.J.M.; Ahmed, Z.Y. 3D concrete printing—A structural engineering perspective. In *High Tech Concrete: Where Technology and Engineering Meet, Proceedings of the 2017 Fib Symposium, Maastricht, The Netherlands, 12–17 June 2017*; Luković, M., Hordijk, D.A., Eds.; Springer: Berlin, Germany, 2017. [CrossRef]
20. Youtube. Available online: https://www.youtube.com/watch?v=8_m-fmkuuUA (accessed on 17 July 2017).
21. Wu, P.; Wang, J.; Wang, X. A critical review of the use of 3-D printing in the construction industry. *Autom. Constr.* **2016**, *68*, 21–31. [CrossRef]
22. Lim, S.; Buswell, R.; Le, T.; Austin, S.; Gibb, A.; Thorpe, T. Developments in construction-scale additive manufacturing processes. *Autom. Constr.* **2012**, *21*, 262–268. [CrossRef]
23. Borg Costanzi, C.; Ahmed, Z.; Schipper, R.; Bos, F.; Knaack, U.; Wolfs, R. 3D Printing concrete on temporary surfaces: The design and fabrication of a concrete shell structure. *Autom. Constr.* **2017**, under review.
24. Huashangluhai. Available online: www.hstdgm.com (accessed on 14 July 2017).
25. Khoshnevis, B.; Hwang, D.; Yao, K.-T.; Yeh, Z. Mega-scale fabrication by contour crafting. *Int. J. Ind. Syst. Eng.* **2006**, *1*, 301–320. [CrossRef]
26. Hambach, M.; Volkmer, D. Properties of 3D-printed fiber-reinforced Portland cement paste. *Cem. Concr. Compos.* **2017**, *79*, 62–70. [CrossRef]
27. 4TU. Available online: <https://www.4tu.nl/bouw/en/lighthouse2017/3D%20Concrete%20Printing%20for%20Structural%20Applications/> (accessed on 26 September 2017).
28. Hack, N.; Lauer, W.V. Mesh-mould: Robotically fabricated spatial meshes as reinforced concrete formwork. *Archit. Des.* **2014**, *84*, 44–53. [CrossRef]
29. Hack, N.; Lauer, W.V.; Gramazio, F.; Kohler, M. Mesh Mould: Robotically fabricated metal meshes as concrete formwork and reinforcement. In *Proceedings of the 11th International Symposium on Ferrocement and 3rd ICTRC International Conference on Textile Reinforced Concrete, Aachen, Germany, 7–10 June 2015*.
30. Bos, F.P.; Ahmed, Z.Y.; Wolfs, R.J.M.; Salet, T.A.M. 3D printing concrete with reinforcement. In *High Tech Concrete: Where Technology and Engineering Meet, Proceedings of the 2017 Fib Symposium, Maastricht, The Netherlands, 12–14 June 2017*; Luković, M., Hordijk, D.A., Eds.; Springer: Berlin, Germany, 2017; pp. 2484–2493. [CrossRef]
31. Bos, F.; Wolfs, R.; Ahmed, Z.; Salet, T. Additive manufacturing of concrete in construction: Potentials and challenges of 3D concrete printing. *Virtual Phys. Prototyp.* **2016**, *11*, 209–225. [CrossRef]
32. Hagan, P.; Chen, J.; Saydam, S. The Load Transfer Mechanism of Fully Grouted Cable Bolts under Laboratory Tests. In *Proceedings of the Coal Operators' Conference, Wollongong, Australia, 12–14 February 2014*.
33. Chen, J.; Hagan, P.C.; Saydam, S. Sample Diameter Effect on Bonding Capacity of Fully Grouted Cable Bolts. *Tunn. Undergr. Space Technol.* **2017**, *68*, 238–243. [CrossRef]

34. Benmokrane, B.; Chennouf, A.; Mitri, H.S. Laboratory evaluation of cement-based grouts and grouted rock anchors. *Int. J. Rock Mech. Min. Sci. Geomech. Abstr.* **1995**, *32*, 633–642. [[CrossRef](#)]
35. Haskett, M.; Oehlers, D.J.; Mohamed Ali, M.S. Local and global bond characteristics of steel reinforcing bars. *Eng. Struct.* **2008**, *30*, 376–383. [[CrossRef](#)]
36. Fédération Internationale du Béton. *Bond of Reinforcement in Concrete, State-of-Art-Report*; International Federation for Structural Concrete: Lausanne, Switzerland, 2000; ISBN 978-2-88-394050-5.
37. Cairns, J. Bond and anchorage of embedded steel reinforcement in Fib Model Code 2010. *Struct. Concr.* **2015**, *45*–55. [[CrossRef](#)]
38. NEN-EN 1992-1-1 Eurocode 2. *Ontwerp en Berekening van Betonconstructies, Deel 1-1: Algemene Regels en Regels Voor Gebouwen*; Nederlands Normalisatie Instituut: Delft, The Netherlands, 2011.
39. Melo, J.; Rossetto, T.; Varum, H. Experimental, Experimental study of bond–slip in RC structural elements with plain bars. *Mater. Struct.* **2015**, *48*, 2367–2381. [[CrossRef](#)]
40. Abrams, D. Tests of bond between concrete and steel. In *Bulletin No. 71*; Engineering Experiment Station, University Illinois Bull: Carbondale, IL, USA, 1913.
41. Fabbrocino, G.; Verderame, G.M.; Manfredi, G. Experimental behaviour of anchored smooth rebars in old type reinforced concrete buildings. *Eng. Struct.* **2005**, *27*, 1575–1585. [[CrossRef](#)]
42. Verderame, G.M.; Ricci, P.; De Carlo, G.; Manfredi, G. Cyclic bond behaviour of plain bars. Part I: Experimental investigation. *Constr. Build. Mater.* **2009**, *23*, 3499–3511. [[CrossRef](#)]
43. Yeomans, S.R. Galvanized Steel Reinforcement. In *Corrosion of Steel in Concrete Structures*; Poursaee, A., Ed.; Elsevier: Amsterdam, The Netherlands, 2016; ISBN 978-1-78-242381-2. [[CrossRef](#)]
44. ISO 14657. *Zinc-Coated Steel for the Reinforcement of Concrete*; International Organization for Standardization: Geneva, Switzerland, 2005.
45. ASTM A767/A767M-16. *Standard Specification for Zinc-Coated (Galvanized) Steel Bars for Concrete Reinforcement*; ASTM International: West Conshohocken, PA, USA, 2016. [[CrossRef](#)]
46. Swamy, R. Design for durability with galvanized reinforcement. In *Galvanized Steel Reinforcement in Concrete*; Yeomans, S., Ed.; Elsevier: Oxford, UK, 2004; ISBN 978-0-08-044511-3.
47. Kayali, O.; Yeomans, S. Bond of ribbed galvanized reinforcing steel in concrete. *Cem. Concr. Compos.* **2000**, *22*, 459–467. [[CrossRef](#)]
48. Hamad, B.; Mike, J. Bond strength of hot-dip galvanized reinforcement in normal strength concrete structures. *Constr. Build. Mater.* **2005**, *19*, 275–283. [[CrossRef](#)]
49. Pernicova, R.; Dobias, D.; Pokorný, P. Problems connected with use of hot-dip galvanized reinforcement in concrete elements. *Procedia Eng.* **2017**, *172*, 859–866. [[CrossRef](#)]
50. NEN-EN 10080:2005. *Steel for the Reinforcement of Concrete—Weldable Reinforcing Steel—General*; Nederlands Normalisatie Instituut: Delft, The Netherlands, 2005.
51. Banthia, N. A study of some factors affecting the fiber–matrix bond in steel fiber reinforced concrete. *Can. J. Civ. Eng.* **1990**, *17*, 610–620. [[CrossRef](#)]
52. Chanvillard, G.; Aïtcin, P.-C. Pull-out behavior of corrugated steel fibers: Qualitative and statistical analysis. *Adv. Cem. Based Mater.* **1996**, *4*, 28–41. [[CrossRef](#)]
53. Robins, P.; Austin, S.; Jones, P. Pull-out behaviour of hooked steel fibres. *Mater. Struct.* **2002**, *35*, 434–442. [[CrossRef](#)]
54. Soetens, T.; van Gysel, A.; Matthys, S.; Taerwe, L. A semi-analytical model to predict the pull-out behaviour of inclined hooked-end steel fibres. *Constr. Build. Mater.* **2013**, *43*, 253–265. [[CrossRef](#)]
55. He, Q.; Liu, C.; Yu, X. Improving steel fiber reinforced concrete pull-out strength with nanoscale iron oxide coating. *Constr. Build. Mater.* **2015**, *79*, 311–317. [[CrossRef](#)]

